International Journal of Thermophysics, Vol. 20, No. 5, 1999

Isochoric Heat Capacity of Heavy Water at Subcritical and Supercritical Conditions

B. A. Mursalov,[1] I. M. Abdulagatov,[1–3] V. I. Dvoryanchikov,[1] A. N. Kamalov,[1] and S. B. Kiselev[2, 4]

Received January 8, 1999

The heat capacity of heavy water was measured in the temperature range from 294 to 746 K and at densities between 52 and 1105 $kg \cdot m^{-3}$ using a high-temperature, high-pressure adiabatic calorimeter. The measurements were performed at 14 liquid and 9 vapor densities between 52 and 1105 $kg \cdot m^{-3}$. Uncertainties of the measurements are estimated to be within 3% for vapor isochores and 1.5% for the liquid isochores. In the region of the immediate vicinity of the critical point ($0.97 \leqslant T/T_c \leqslant 1.03$ and $0.75 \leqslant \rho/\rho_c \leqslant 1.25$), the uncertainty is 4.5%. The original C_V data were corrected and converted to the new ITS-90 temperature scale. A parametric crossover equation of state was used to represent the isochoric heat capacity measurements of heavy water in the extended critical region, $0.8 \leqslant T/T_c \leqslant 1.5$ and $0.35 \leqslant \rho/\rho_c \leqslant 1.65$. The liquid and vapor one- and two-phase isochoric heat capacities, temperatures, and saturation densities were extracted from experimental data for each measured isochore. Most of the experimental data are compared with the Hill equation of state, and the overall statistics of deviations between experimental data and the equation of state are given.

KEY WORDS: coexistence curve; critical point; crossover equation of state; heavy water; isochoric heat capacity; water.

[1] Institute for Geothermal Problems of the Dagestan Scientific Center of the Russian Academy of Sciences, 367030 Makhachkala, Kalinina 39-A, Dagestan, Russia.

[2] Guest researcher at the Physical and Chemical Properties Division, National Institute of Standards and Technology, 325 Broadway, Boulder, Colorado 80303, U.S.A.

[3] To whom correspondence should be addressed.

[4] Present address: Chemical Engineering and Petroleum Refining Depertment, Colorado School of Mines, Golden, Colorado 80401, U.S.A.

0195-928X/99/0900-1497$16.00/0

1. INTRODUCTION

Isochoric heat capacity measurements are useful in developing equations of state because they yield valuable information about the second derivative of the pressure and of the Helmholtz energy with respect to temperature. Detailed comparisons of experimental C_V data with available equations of state are needed to establish their accuracy. C_V experiments contain direct information on the curvature behavior of the P–T isochores, which are extremely important in the development of a reliable equation of state (EOS).

In this work, we present the results of C_V measurements of heavy water obtained by Mursalov in 1973 [1]. The complete results have not been published until now. Previously [2], the C_V data of heavy water were published for two isochores, 303 and 345 $kg \cdot m^{-3}$. In this work, we have collected all the unpublished isochoric heat capacity data of heavy water measured by Mursalov. These data have been evaluated, sources of uncertainties were assessed, and the data were corrected when required and converted to the ITS-90 temperature scale. The heat capacity at constant volume, C_V, of heavy water has been measured in this work in the temperature range from 294 to 746 K and at densities between 52 and 1105 $kg \cdot m^{-3}$ in the one- and two-phase regions. These regions include saturation as well as subcritical and supercritical conditions. The measurements were made in a high-temperature, high-pressure, adiabatic, and nearly constant-volume calorimeter. These experimental results contribute to the development of models of the crossover behavior of C_V. Detailed comparisons with the Hill et al. [3] EOS, additionally described by Kestin and Sengers [4], and overall statistics are presented. An application of the parametric crossover equation of state proposed by Kiselev et al. [5] to these data is presented.

2. EXPERIMENTAL

For studying the heat capacities of liquids, gases, and their mixtures at constant volume, including near the critical point, the following requirements are usually imposed on the measuring system: (1) the calorimeter should reliably ensure adiabatic conditions, (2) the heat capacity of the empty calorimeter should be small in comparison with that of the substance to be studied, and (3) the system should operate over a wide range of state conditions. Near the critical point, additional features must be considered, such as the sensitivity of a substance to external disturbances and the difficulty of achieving a homogeneous equilibrium state. This leads to additional restrictions on the experimental apparatus: (4) the temperature step should be small, (5) the system should ensure stable operation for a long period, and (6) gravitational effects must be reduced to a minimum.

These requirements are satisfied by the high-temperature, high-pressure, integrating adiabatic calorimeter used in this work. The main ideas underlying this method, which is intended for experimental studies of heat capacity at constant volume of liquids and gases over a wide range of temperatures (from room temperature to 1000°C) and pressures (to 100 MPa), including the critical region, were formulated by Amirkhanov et al. [6, 7]. These ideas were realized in practice and successfully employed for experimental measurements of C_V for various fluids and fluid mixtures in the extended critical region [8–18].

2.1. Principle of the Method

If a layer of a semiconductor is placed between two concentric spherical vessels, the system will behave as a highly sensitive thermoelement that can serve as a sensor detecting deviations from adiabatic conditions. In such a calorimeter, only the inner thin-walled vessel and the adjacent portion of the semiconductor layer contribute to the heat capacity of the calorimeter itself. The semiconductor layer simultaneously plays the role of a buffer that transmits pressure from the thin inner shell to the thicker outer shell. This makes it possible to increase the strength of the calorimeter without increasing its heat capacity. Adiabatic conditions are reliably maintained in this calorimeter.

The walls of the inner vessel are maintained at a temperature T, and the walls of the outer vessel are maintained at a higher temperature $T+\Delta T$. The intensity of the electric field in the semiconductor layer is determined by the relationship [7]

$$\varepsilon = \alpha \operatorname{grad} T \tag{1}$$

where α is the thermoelectric power, which depends on the nature of the semiconductor material and temperature T. When the outer and the inner shells of the calorimeter are connected through a sensitive galvanometer, a direct current I, which is caused by the thermal emf, passes through the circuit [7],

$$dI = \alpha\, dT \tag{2}$$

From the value of this current, the magnitude of the temperature gradient between the calorimeter shells can be calculated. Cuprous oxide (Cu_2O) has a very high α (about 1150 $\mu V \cdot K^{-1}$) in comparison with other semiconductors. This makes it possible to detect extremely small temperature differences. Temperature differences between the shells as small as 10^{-6} K may be detected by connecting the leads from the calorimeter shells to a

potentiometer. This makes it possible to almost eliminate heat transfer through the semiconductor layer during the whole cycle of measurements. In this case, the heat that is released by the heater located in the calorimeter is used only to heat the substance located inside the inner thin-walled shell of the calorimeter and a thin layer of cuprous oxide that directly adjoins the inner shell. The rest of the system is heated by an external heater. Thus, only the heat capacities of the sample, located in the inner shell of the calorimeter, and of the adjacent portion of the semiconductor layer take part in the thermal balance of the calorimetric system. If a solid semiconductor tightly fills the gap between the concentric shells, heat exchange between the calorimeter and the shell occurs only by thermal conduction. If a liquid or a vacuum is used between the shells, heat losses are caused not only by thermal conduction, but also by convection and radiation. Since cuprous oxide has a low thermal conductivity ($\lambda \approx 2.09$ $W \cdot m^{-1} \cdot K^{-1}$), the use of this semiconductor leads to only small heat losses.

A layer of a fine powder semiconductor material uniformly filling the gap between the concentric shells acts as an adiabatic integrating regulator. If the temperature field at the surface of the calorimeter becomes nonuniform, conditions can easily be made such that the net emf in the thermoelement circuit becomes zero. Since the thermal emf is caused by the temperature gradients existing in the bulk of the semiconductor, which may not be zero at all points of the surface due to the nonuniform temperature field, the net thermal emf is [7]

$$\int_S \mathscr{E}\, dS = \alpha \int_S \operatorname{grad} T\, dS \tag{3}$$

and may be zero even if there are regions where the local temperature gradients (grad T) have opposite signs. The heat flux through a unit area of the semiconductor surface layer per unit time is

$$q = \lambda \cdot \operatorname{grad} T \tag{4}$$

where λ is the thermal conductivity of the semiconductor layer. The heat flux through the whole surface is [7]

$$Q = \int_S q\, dS = \int_S \lambda \operatorname{grad} T\, dS = \frac{\lambda}{\alpha} \int_S \mathscr{E}\, dS \tag{5}$$

For a homogeneous substance (semiconductor layer), λ and α are the same at all points and thus the net heat flux through the thermoelement is zero ($Q = 0$).

2.2. Construction of the Calorimeter

The details of the construction of the calorimeter are given in several papers [7–11]. A schematic of the C_V calorimeter is presented in Fig. 1. The calorimeter is a multilayered system which consists of an internal thin-walled vessel (1), outer adiabatic shells (3–5), and a semiconductor layer (2) between them. The inner vessel (1) is made of 1X18H9T stainless steel and has walls 0.5 to 0.8 mm thick. Cylindrical wells are used for an internal heater (6), a resistance thermometer (8), and measuring thermocouples. The outer shell (3) is made of the same steel but has walls 8 mm thick. The heater of the outer shell (3) is made of a copper wire (0.18 mm in diameter in a glass-fiber insulation) double-wound on the surface of the shell. In order to improve thermal contact, the heater is cemented to the surface of the shell with K-47 lacquer. This helps to improve the isothermal conditions of the external surface of the calorimeter.

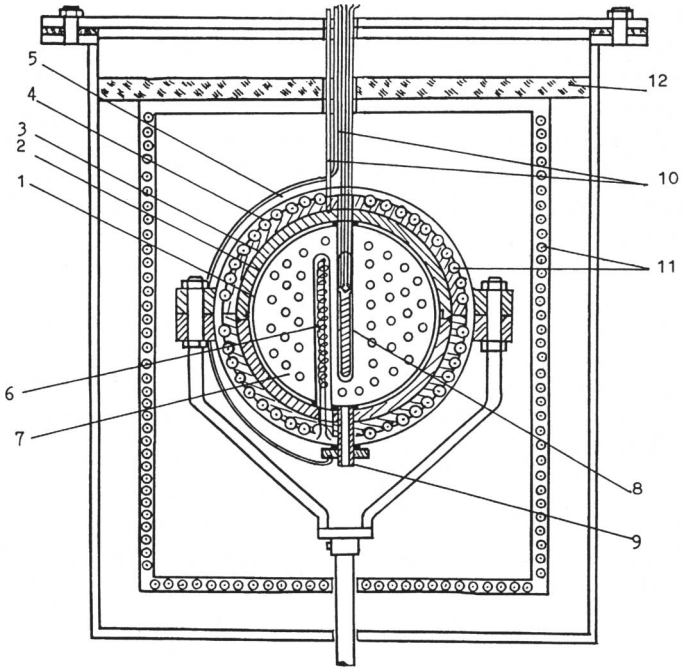

Fig. 1. Schematic representation of the apparatus for C_V measurements: (1) inner thin-walled spherical vessel; (2) semiconductor layer of Cu_2O; (3–5) outer shells; (6) inner heater; (7) perforated stirrer; (8) PRT-10; (9) filling pipe; (10) steel tap; (11) outer heaters; (12) asbestos gasket.

A thermoelement [semiconductor layer (2)] of cuprous oxide was used. It has a thermal emf of about 1150 $\mu V \cdot K^{-1}$, which is almost independent of temperature between 350 and 750 K. Cuprous oxide has a low thermal conductivity and serves as a heat-insulating layer, which greatly decreases heat losses. Simultaneously, the cuprous oxide layer plays the role of a differentiating medium transmitting pressure to the stronger outer shells (3–5). The out-of-balance signal from the integrating thermoelement (cuprous oxide) was first applied to the input of an amplifying microvoltmeter, whose output feeds a high-precision temperature regulator (HPTR). The circuit used for controlling adiabatic conditions in the system enabled the out-of-balance temperature to be maintained within 10^{-5} K.

The calorimeter was mounted using four studs in a ring of a rotating-oscillating mechanism that can be used to mix the liquid in the calorimeter. A thermal shield decreased convective flows and improved the uniformity of the temperature field in the thermostat. This shield (made of aluminum) consisted of two hemispheres 150 mm in diameter with walls 3 mm thick. The heater of the shield was made of a constantan wire (0.2 mm in diameter, covered with a glass-fiber insulation) wound onto the whole surface and cemented with a lacquer. The sensor of the temperature difference (out-of-balance signal) between the calorimeter shell and the shield consisted of a five-junction copper–constantan thermopile whose signal was fed to an R-363/2 potentiometer, and from this potentiometer it was fed to a high-precision temperature regulator. The temperature difference was controlled within 5×10^{-3} K.

The calorimeter and the shield were placed in a spherical thermostat which consisted of two massive hemispheres made of 20 mm thick aluminum. The heater of the thermostat was made of a constantan wire 0.6 mm in diameter in a glass-fiber insulation 0.5 mm thick and was tightly wrapped onto the whole surface of the thermostat. To improve the electric insulation, the surface of the thermostat was covered with a heat-resistant lacquer. The heater was powered by an HPTR, and the temperature changes were controlled with a differential thermocouple connected to an R-348 potentiometer. A differential copper–constantan thermocouple made of wires 0.15 to 0.30 mm in diameter in a glass-fiber insulation was used as a temperature sensor. In order to improve thermal contact, the thermocouple junctions were caulked into the channels of the thermostat and shield and were insulated with a lacquer. The circuit was controlled by proportional-integral regulation and maintained a desired temperature to within 0.1 K in the range between 300 and 700 K.

The spherical thermostat, in turn, was placed in a protective jacket. When making measurements near the critical point, the sample was vigorously mixed using a stirrer made of a thin perforated foil of stainless

steel. The mixing was performed by rotating the calorimeter about the vertical axis. The temperature of the sample was measured by a miniature standard resistance thermometer (Type PTS-10; $R_0 = 10.1230\ \Omega$, $R_{100}/R_0 = 1.39238$).

2.3. Heat Capacity of the Empty Calorimeter

The heat capacity of the empty calorimeter C_0 was determined experimentally using standard substances (water and nitrobenzene) with well known isobaric heat capacities at atmospheric pressure in the temperature range up to 423 K [12, 13] with a correction for the temperature dependence of the heat capacity of the material of the calorimeter. At higher temperatures ($T > 423$ K) the value of C_0 was determined by using the isobaric heat capacity at atmospheric pressure of air [14]. The uncertainty of C_0 measurements is 0.5 to 1.5%, depending on the temperature range. For measurements of the isochoric heat capacity of heavy water, two calorimetric vessels made from stainless steel and platinum with volumes at 293 K of 100.58 ± 0.05 cm^3 and 413.92 ± 0.03 cm^3 were used. The values of the empty calorimeter heat capacities were 43.96 J · K^{-1} for stainless steel and 128.96 J · K^{-1} for platinum.

The heat capacity of the calorimetric system was also calculated as the sum of the heat capacities of the inner vessel, stirrer, connecting pipes, the layer of cuprous oxide, etc., using the relationship [7, 8]

$$C_0 = mC_1 + \frac{m_0}{1 + \sqrt{r_2^3/r_1^3}} C_2 \tag{6}$$

where m is the mass of the inner shell with the stirrer, m_0 is the mass of cuprous oxide, C_1 and C_2 are the heat capacities of steel and cuprous oxide, respectively, and r_1 and r_2 are the radii of the inner and outer shells of the calorimeter. The calculated values of C_0 were systematically lower than measured values by 4 to 5% because the calorimeter was multilayered.

2.4. Measurement of the Working Volume of the Calorimeter

The working volume of the calorimeter is the volume of its inner shell minus the volumes occupied by the stirrer and wells for both the resistance thermometer and the inner heater. In order to determine the working volume, the calorimeter was thoroughly washed, dried, and weighed on a VLT-1 analytical balance to an accuracy of 0.5 mg. After this, the calorimeter was filled with twice-distilled water and was weighed again. At a given temperature and atmospheric pressure, the volume of the

calorimeter can be found from the density of water. Five or six repetitions at different temperatures were used in each experiment. The uncertainty in determining the working volume of the calorimeter did not exceed 0.04%. Changes in the volume of the calorimeter due to changes in temperature (ΔV_T) and pressure (ΔV_P) were determined both experimentally and by calculation.

Assuming that the inner shell is spherical, the correction for the effect of pressure was calculated by the formula

$$\Delta V_P = V_0[3(1-2\mu)(P-P_0n^3) + 1.5(1+\mu)(P-P_0)\,n^3]/E(n^3-1) \qquad (7)$$

where $\mu = 0.3$ is Poisson's ratio for steel, $E = 2.0265 \times 10^5$ MPa is the Young's modulus of the steel, P is the working pressure in the vessel, P_0 is the ambient pressure, $n^2 = R/r$, R is the outer radius, and r is the inner radius of the sphere.

Since the calorimeter represents a multilayered (nonuniform) sphere consisting of layers of steel, cuprous oxide, and again steel, the validity of Eq. (7) in calculating the change in volume at a specified pressure was specially tested in Ref. 15 for the calorimeter with $V_0 = 400.99$ cm^3. At 5 MPa, the correction for the pressure effect was 0.065 cm^3. The difference between Eq. (7) and the actual expansion was 20%. The error in the determination of the calorimeter volume with corrections for ΔV_T and ΔV_P varies between 0.05 and 0.09% in the temperature range of 300 to 600 K.

2.5. Preparation of the Calorimeter and the Technique of Measurements

Before the experiments were run, the calorimeter was thoroughly washed with a special solution consisting of 77% H_2O, 2% $KClO_4$, 1% NaCl, and 20% H_2SO_4 by mass. The solution was warmed to 40 to 50°C, poured into the calorimeter vessel, and intensely shaken. Then, the calorimeter was rinsed with hot flowing distilled water for 5 to 8 h. After the washing was completed, the calorimeter was weighed and filled with the liquid to be studied, using a special apparatus [8]. Before it was filled, the calorimeter vessel was carefully evacuated and the calorimeter was filled with the substance to be studied and was again weighed. The mass of the substance in the calorimeter was determined by the difference in the weights of the empty and full calorimeter.

Measurements of C_V were carried out at constant volume by the continuous-heating method. This method enables one to determine, to a good accuracy, the transition temperature T_s of the system from the two-phase to a single-phase state (i.e., to determine T_s and ρ_s data corresponding to

the phase coexistence curve), the jump in the heat capacity ΔC_V, and reliable C_V data in the single- and two-phase regions.

After the heaters of the thermostat, shield, and external jacket were switched on, the system was brought to the desired temperature. The desired temperature was adjusted and controlled automatically. In the calorimeter, three thermocouples were placed at different depths. The thermal control was established so that all three thermocouples showed the same temperature, which indicated that the system had reached thermodynamic equilibrium. A constant thermoelectric potential difference was established across the layer of cuprous oxide; this difference ensures the absence of heat exchange between the calorimeter and the jacket. Switching on the internal heater disturbed the equilibrium of the heat exchange process for a few minutes, but it was restored quickly by automatically controlling the power supplied to the external jacket of the calorimeter. The rate of temperature change, determined by the power supplied to the internal heater, varied from 5×10^{-4} to 8×10^{-5} K · s^{-1}, depending on the region where the investigation was carried out. Near the critical point and the phase transition curve, the measurements were performed using minimal rates.

In the region of regular behavior of C_V, the measurements were carried out in temperature steps of 0.15 to 0.20 K; in the region of critical anomalies, the step was decreased to 0.02 to 0.05 K. The heat capacity C_V is calculated by the expression

$$C_V = \frac{1}{m}\left\{\frac{\Delta Q}{\Delta T} - C_0\right\} \tag{8}$$

where m is the mass of the sample in the calorimeter, $\Delta Q = IU\tau$ is the amount of heat released by the internal heater, I is the current passing through the internal heater, U is the voltage drop, τ is the time of heating, and C_0 is the heat capacity of the empty calorimeter.

2.6. Uncertainties in Measuring C_V

The uncertainty in C_V measurements arises from several sources. The heat capacity experiment was subjected to two general types of uncertainties: measurement errors and nonmeasurement errors. Measurement uncertainties were associated with uncertainties that exist in measured quantities contained in Eq. (8) used to compute C_V from experimental data. Nonmeasurement errors were associated with deviations of actual experimental conditions from the mathematical model used to derive the equation for computing the heat capacity.

The heat capacity was obtained from the measured quantities m, I, U, τ, ΔT, and C_0. The accuracy of the heat capacity measurements was assessed by analyzing the sensitivity of Eq. (8) to the experimental uncertainties of the measured quantities. The maximum relative uncertainty of C_V associated with m, I, U, τ, ΔT, and C_0 measurements can be estimated from the equation

$$\frac{\delta C_V}{C_V} = \delta m + \{q\delta C_0 + q\delta(\Delta T) + q[\delta I + \delta U + \delta\tau] + [\delta I + \delta U + \delta\tau + \delta(\Delta T)]\} \tag{9}$$

where $q = C_0/(mC_V)$ is the factor which depends on the ratio of the empty calorimeter heat capacity C_0 to the product of the heat capacity of the sample C_V and the mass of the sample m. The terms δm, δI, δU, $\delta\tau$, $\delta(\Delta T)$, and δC_0 are the relative uncertainties of measured quantities. The heating time τ of the experiment was measured with an F-5041 frequency meter with an accuracy of 0.01 s. The relative uncertainty in determining the supplied amount of heat ΔQ was $\delta(\Delta Q) = \delta I + \delta U + \delta\tau \approx 0.08\%$ ($\delta I = 0.02\%$, $\delta U = 0.06\%$, and $\delta\tau = 0.003\%$). The relative uncertainty $\delta(\Delta T)$ in determining the temperature difference depended on the magnitude of this difference. In the region where the heat capacity changes sharply (near the phase transition and critical points) and ΔT was small (0.02 to 0.05 K), the uncertainty in determining ΔT was 0.5%. In the region where the heat capacity does not change rapidly (far from phase transition and critical points) and ΔT was 0.5 to 1.0 K, the measurement uncertainty was about 0.05%. The relative uncertainty in determining the mass m of the sample was 0.01%. The temperature was measured with a PRT (PTS-10) mounted in a tube inside the calorimetric sphere. The thermometer was calibrated on IPTS-68. The uncertainty of temperature measurements was less than 10 mK. The density of the sample was determined as the ratio of the mass of the sample m to the working volume V_{PT} of the calorimetric vessel, $\rho = m/V_{PT}$. The volume V_{PT} of the calorimeter was corrected for its variation with temperature T and pressure P (see Section 2.4). The average value of the working volume was determined with an uncertainty that did not exceed 0.04%. The sample density also changed because of the temperature- and pressure-related changes of the calorimeter volume during heat capacity measurements. Thus, the measurements were actually performed along quasi-isochores.

In Eq. (9), the major measurement uncertainties are associated with the terms $q\delta C_0$, $q\delta(\Delta T)$, and $\delta(\Delta T)$, which represent the uncertainties involved in the measured empty calorimeter heat capacity C_0 and temperature difference ΔT. As the factor q increased, the uncertainty in C_V

measurements increased linearly. Therefore, the calorimeter must be designed with the condition $q \ll 1$, that is, $C_0 \ll mC_V$. The uncertainty in C_V measurements depends on the mass m of the measured sample. Therefore, for the vapor isochores (small m) the uncertainty in C_V measurements is large and for the liquid isochores (large m) the uncertainty in C_V measurements is lower. For our construction of the calorimeter, the values of q fell in the range from 0.15 to 0.9.

At a selected experimental temperature T and density ρ, the measurements of C_V were performed with different temperature differences ΔT (from 0.03 to 0.5 K) and energy differences ΔQ (from 400 to 820 J). The measured heat capacities were indeed independent of the applied temperature differences and power differences. The measurements agreed within 0.3% when the applied temperature and power differences varied by a factor of 3. All measurements were made with the samples vigorously stirred using a stirrer made of a thin perforated steel foil. This permitted reduction of the errors caused by gravity and achieved homogenization of the sample.

The major sources of nonmeasurement (systematic) uncertainties included the following: (1) the nonisochoric behavior of the apparatus (deviations of the system from a constant volume) during heating, (2) the nonadiabatic conditions of the system, (3) stray heat flows through the calorimeter not controlled by the semiconductor layer, e.g., parasitic flows caused by spurious temperature differences, and (4) random errors that lead to scatter in experimental data.

The correction related to the nonisochoric behavior during heating was determined by the relation [10]

$$C_V = C_V^{\exp} - T\left(\frac{\partial P}{\partial T}\right)_V \left\{\left(\frac{dV}{dT}\right) + \left(\frac{\partial P}{\partial T}\right)_V \frac{dV}{dP}\right\}\left\{1 - \frac{dV}{dP}\left(\frac{\partial P}{\partial V}\right)_T\right\}^{-1} \tag{10}$$

where the partial derivatives refer to the sample under study and the ordinary derivatives refer to the calorimeter. This correction was determined to an uncertainty of 5%, which constitutes 0.5 to 1.0% of the total magnitude of the heat capacity in the temperature range from 300 to 650 K.

The possible supply or removal of heat through the layer of the thermoelement caused by the imperfect adiabatic behavior of the system was determined from the relation [7]

$$\Delta Q = \lambda \frac{\Delta T}{d} S\tau \tag{11}$$

Table I. Experimental Values of the Isochoric Heat Capacities of Heavy Water in the Single- and Two-Phase Regions ($T = T_{exp} - 0.45$ K)

T (K)	C_V (kJ · kg^{-1} · K^{-1})	T (K)	C_V (kJ · kg^{-1} · K^{-1})	T (K)	C_V (kJ · kg^{-1} · K^{-1})
$\rho = 1104.97$ kg · m^{-3}		346.880	3.831	422.515	3.492
293.835	4.204[a]	347.090	3.839	422.895	3.500
294.075	4.208[a]	347.530	3.814	425.604	3.496
294.315	4.195[a]	347.690	3.772	426.374	3.467
294.555	4.208[a]	355.758	3.693	426.754	3.454
295.044	4.183	356.838	3.689	442.862	3.308
295.294	4.174	357.488	3.693	444.002	3.337
295.524	4.170	366.425	3.626	444.572	3.316
295.764	4.174	367.055	3.622	446.462	3.282
302.492	4.128	367.475	3.634	446.852	3.253
302.722	4.132	$\rho = 1063.83$ kg · m^{-3}		447.412	3.262
302.962	4.124	369.585	4.204[a]	455.871	3.220
303.202	4.137	370.634	4.208[a]	456.621	3.228
312.610	4.044	371.464	4.216	456.991	3.215
312.840	4.053	372.094	4.212	$\rho = 1008.06$ kg · m^{-3}	
313.079	4.049	372.514	3.756	427.724	4.197[a]
317.488	4.061	372.934	3.735	428.114	4.188[a]
317.718	4.044	373.084	3.751	428.494	4.213[a]
317.948	4.019	373.564	3.747	428.884	4.197[a]
322.537	3.994	374.393	3.751	429.654	4.197[a]
322.767	3.986	376.893	3.622	430.234	4.213[a]
322.997	3.998	377.313	3.630	430.624	4.222[a]
332.734	3.877	377.723	3.634	431.004	4.226[a]
332.954	3.844	396.959	3.567	431.393	3.444
333.174	3.827	397.559	3.538	431.583	3.478
342.501	3.806	398.568	3.509	432.543	3.465
342.721	3.751	398.968	3.509	433.893	3.457
342.941	3.768	406.767	3.442	434.463	3.453
$\rho = 1095.29$ kg · m^{-3}		407.757	3.429	435.233	3.428
321.617	4.191[a]	408.947	3.416	436.193	3.415
322.307	4.187[a]	409.736	3.416	436.763	3.440
322.767	4.195[a]	415.466	3.391	445.522	3.315
323.227	4.204	416.245	3.358	446.282	3.294
323.677	4.195	417.035	3.341	446.662	3.273
323.907	4.032	417.625	3.379	447.602	3.298
324.136	4.044	$\rho = 1017.29$ kg · m^{-3}		447.982	3.269
324.596	4.036	418.805	4.250[a]	455.861	3.214
324.816	4.019	419.585	4.262[a]	456.431	3.223
339.412	3.957	420.565	4.262[a]	456.811	3.210
340.082	3.944	421.535	4.271[a]	457.931	3.260
340.522	3.944	422.125	4.262[a]	458.301	3.219
346.440	3.844			466.861	3.181

Table I. *(Continued)*

T (K)	C_V (kJ · kg^{-1} · K^{-1})	T (K)	C_V (kJ · kg^{-1} · K^{-1})	T (K)	C_V (kJ · kg^{-1} · K^{-1})
467.411	3.156	504.290	3.118	546.931	4.656[a]
467.971	3.143	504.650	3.106	547.791	4.627[a]
468.151	3.143	508.060	3.081	548.831	4.644[a]
468.521	3.127	508.240	3.093	549.521	4.652[a]
468.891	3.143	516.800	3.043	549.861	4.661[a]
$\rho = 957.85$ kg · m^{-3}		517.680	3.030	550.161	2.976
		518.560	3.030	550.721	2.984
469.081	4.312[a]	518.920	3.001	551.071	2.943
469.451	4.346[a]	519.100	2.989	552.961	2.943
469.821	4.359[a]	525.810	2.926	553.481	2.951
470.930	4.350[a]	526.160	2.930	553.991	2.959
471.850	4.359[a]	527.920	2.897	555.371	2.984
472.220	4.379[a]	528.970	2.918	555.541	2.947
472.400	4.371[a]	529.150	2.964	566.491	2.867
472.770	3.266	531.260	2.947	566.831	2.822
473.140	3.266	532.120	2.930	567.341	2.830
473.690	3.278	532.650	2.938	568.871	2.809
474.240	3.224	$\rho = 882.61$ kg · m^{-3}		571.041	2.846
490.600	3.107			570.911	2.813
491.500	3.132	519.630	4.572[a]	571.251	2.838
492.220	3.102	519.980	4.572[a]	585.091	2.750
492.590	3.077	520.870	4.580[a]	585.421	2.721
499.790	2.981	521.930	4.589[a]	585.591	2.684
505.370	2.973	522.560	4.585[a]	588.951	2.742
506.810	2.964	522.990	3.065	589.141	2.692
$\rho = 925.93$ kg · m^{-3}		524.580	3.069	589.291	2.730
		526.510	3.065	589.791	2.721
492.950	4.293[a]	527.040	3.056	589.961	2.725
493.310	4.289[a]	527.740	3.048	592.801	2.721
493.850	4.322[a]	542.581	2.922	593.131	2.654
494.030	4.339[a]	543.101	2.918	593.301	2.667
495.830	4.330[a]	543.621	2.893	$\rho = 783.70$ kg · m^{-3}	
496.010	4.330[a]	543.971	2.889		
496.550	4.339[a]	546.231	2.872	569.891	4.928[a]
496.910	4.347[a]	546.751	2.860	570.061	4.936[a]
497.270	4.351[a]	547.441	2.839	570.741	4.940[a]
497.450	3.198	550.551	2.830	571.251	4.953[a]
497.810	3.194	556.921	2.780	571.931	4.945[a]
498.890	3.206	557.771	2.772	572.611	4.953[a]
499.610	3.173	$\rho = 833.33$ kg · m^{-3}		572.951	2.901
499.790	3.202			573.121	2.860
503.930	3.156	545.021	4.623[a]	573.791	2.864
504.110	3.131	545.891	4.636[a]	585.421	2.855

Table I. *(Continued)*

T (K)	C_V (kJ · kg^{-1} · K^{-1})	T (K)	C_V (kJ · kg^{-1} · K^{-1})	T (K)	C_V (kJ · kg^{-1} · K^{-1})
586.271	2.839	643.757	3.065	647.626	4.304
587.441	2.843	646.656	3.073	647.786	4.082
604.560	2.663	647.626	3.073	647.946	4.040
605.610	2.659	652.125	2.998	648.106	3.977
606.770	2.671	652.445	2.973	648.266	4.032
610.070	2.680	676.621	2.851	648.426	3.998
610.730	2.646	677.561	2.860	648.596	3.994
616.829	2.587	678.980	2.847	651.805	3.977
617.489	2.596	681.490	2.847	651.965	3.957
$\rho = 667.56$ kg · m^{-3}		682.430	2.826	652.125	3.852
		695.696	2.814	652.285	3.802
609.240	5.774[a]	696.006	2.809	652.445	3.814
610.070	5.786[a]	696.316	2.839	652.765	3.852
610.560	5.799[a]	702.804	2.839		
611.060	5.824[a]	703.264	2.830	$\rho = 370.37$ kg · m^{-3}	
611.720	5.841[a]	709.242	2.797	642.787	11.886[a]
612.380	2.855	709.862	2.788	643.437	12.560[a]
614.030	2.851	$\rho = 400.00$ kg · m^{-3}		643.597	13.360[a]
614.690	2.855			643.757	14.486[a]
615.350	2.860	641.977	9.847[a]	643.817	15.784[a]
630.288	2.784	642.137	9.935[a]	644.077	8.005
630.778	2.788	642.467	10.287[a]	644.407	6.720
631.748	2.772	642.787	10.438[a]	644.567	6.071
632.568	2.776	642.947	10.969[a]	644.726	6.167
646.816	2.671	643.107	11.346[a]	644.886	5.677
647.466	2.709	643.267	11.974[a]	645.046	5.443
649.876	2.633	643.437	12.351[a]	645.206	5.250
650.206	2.638	643.597	13.071[a]	645.366	5.234
652.445	2.692	643.767	6.376	645.536	5.070
653.885	2.675	643.917	5.640	645.696	4.953
654.525	2.663	644.077	5.422	645.856	4.919
$\rho = 492.61$ kg · m^{-3}		644.247	5.213	646.016	4.819
		644.407	5.129	646.176	4.710
637.927	7.373[a]	644.567	4.986	646.336	4.652
638.737	7.398[a]	644.726	4.823	646.496	4.660
639.707	7.423[a]	644.886	4.731	646.656	4.605
639.867	7.448[a]	645.046	4.605	651.006	4.526
640.197	7.461[a]	645.206	4.585	651.166	4.480
640.677	7.503[a]	645.366	4.522	651.326	4.007
641.007	3.102	645.536	4.467	651.486	3.952
641.327	3.098	645.696	4.375	651.645	3.952
641.487	3.102	645.856	4.451	651.805	3.998
642.137	3.086	647.466	4.325	651.965	3.977

Table I. *(Continued)*

T (K)	C_V (kJ · kg^{-1} · K^{-1})	T (K)	C_V (kJ · kg^{-1} · K^{-1})	T (K)	C_V (kJ · kg^{-1} · K^{-1})
652.125	3.910	652.605	4.021	643.698	16.370[a]
652.285	3.894	652.765	4.067	643.710	18.966[a]
652.445	3.936	664.263	3.545	644.077	7.628
652.605	3.894	664.903	3.499	644.247	6.967
		665.703	3.507	644.407	6.347
$\rho = 344.828$ kg · m^{-3}		672.052	3.490	644.567	6.423
639.707	9.205[a]	672.362	3.465	644.726	6.146
640.197	9.401[a]	672.672	3.436	644.886	5.862
640.837	10.500[a]	678.821	3.240	645.046	5.614
641.327	10.367[a]	679.130	3.240	645.206	5.409
641.497	9.978[a]	679.290	3.194	645.286	5.292
641.817	10.212[a]	679.760	3.202	645.536	5.359
642.137	10.672[a]	683.689	3.152	645.696	5.234
642.307	11.023[a]	683.999	3.181	645.846	5.137
642.787	12.239[a]	685.099	3.131	646.336	5.129
642.947	12.979[a]	690.708	3.185	646.496	5.083
643.107	12.423[a]	690.868	3.148	646.756	4.919
643.267	13.401[a]	695.227	3.072	646.816	4.739
643.427	13.957[a]	695.387	3.039	646.976	4.647
643.597	17.021[a]	695.536	3.047	647.146	4.693
643.757	18.559[a]	695.846	3.010	647.306	4.660
643.917	6.901	698.956	3.068	650.846	4.187
644.077	6.111	699.106	3.010	651.006	4.576
644.727	5.421	699.255	3.026	651.166	4.472
645.047	5.263	699.415	2.993	651.326	4.082
645.217	5.079	707.873	3.026	651.486	4.120
645.536	4.815	708.023	3.030	651.805	4.124
645.696	4.970	710.012	2.888	651.965	4.103
645.856	4.912	710.162	2.892		
646.016	4.882	710.312	2.905	$\rho = 303.03$ kg · m^{-3}	
646.176	4.585	710.472	2.842	642.947	11.297[a]
646.336	4.494	710.932	2.842	643.107	11.765[a]
646.656	4.368	739.423	2.684	643.267	11.924[a]
646.816	4.381	740.453	2.621	643.597	12.460[a]
646.976	4.473	741.472	2.633	643.639	12.824[a]
647.136	4.443	742.492	2.650	643.645	13.975[a]
647.306	4.518			644.087	5.828
647.466	4.494	$\rho = 338.41$ kg · m^{-3}		644.247	5.653
647.626	4.439	642.787	12.351[a]	644.407	5.230
647.786	4.322	643.107	12.812[a]	644.567	4.916
651.806	4.084	643.267	12.895[a]	644.677	4.812
652.126	4.004	643.437	14.068[a]	644.887	4.628
652.445	4.096	643.597	15.198[a]	645.047	4.531

Table I. *(Continued)*

T (K)	C_V (kJ · kg^{-1} · K^{-1})	T (K)	C_V (kJ · kg^{-1} · K^{-1})	T (K)	C_V (kJ · kg^{-1} · K^{-1})
645.207	4.577	669.512	3.429	663.154	3.387
645.367	4.456	689.308	3.098	663.473	3.391
645.526	4.435	689.778	3.094	664.423	3.416
646.496	4.418	690.088	3.102	665.223	3.358
646.666	4.289	690.238	3.052	665.543	3.341
646.816	4.310	690.708	3.090	684.159	3.031
646.976	4.192	691.177	3.056	684.469	2.994
647.136	4.142	704.654	2.914	685.099	3.040
649.076	4.151	704.964	2.889	685.249	3.073
649.236	4.159	705.114	2.868	713.681	2.659
649.396	4.167	705.274	2.864	713.991	2.650
649.636	4.163	705.424	2.897	714.131	2.680
649.876	4.134	705.574	2.897	714.441	2.684
651.646	4.138	705.724	2.851	714.741	2.642
		706.193	2.876	714.901	2.638
$\rho = 261.10$ kg · m^{-3}		722.958	2.747	738.393	2.537
		723.998	2.721	738.653	2.533
641.167	12.753[a]	725.028	2.747	738.913	2.550
641.487	12.774[a]	726.057	2.680	739.173	2.550
641.977	12.761[a]	745.571	2.613		
642.467	12.946[a]	745.841	2.587	$\rho = 170.39$ kg · m^{-3}	
642.787	13.540[a]	746.091	2.587		
642.947	14.101[a]	746.350	2.550	629.798	10.794[a]
643.277	4.333	746.031	2.562	629.958	10.844[a]
643.597	4.258			630.448	10.815[a]
643.757	4.229	$\rho = 219.30$ kg · m^{-3}		630.778	10.990[a]
644.077	4.116			630.938	10.999[a]
644.407	4.082	637.117	10.572[a]	631.588	11.053[a]
644.726	4.099	637.277	10.526[a]	631.918	10.576[a]
645.046	4.070	637.927	10.538[a]	632.078	11.631[a]
659.324	3.718	638.407	10.823[a]	632.238	3.701
659.644	3.676	639.067	10.936[a]	632.568	3.676
659.964	3.680	639.377	11.748[a]	632.728	3.659
660.284	3.718	639.707	4.162	632.898	3.638
660.444	3.668	639.867	3.927	639.227	3.521
660.764	3.676	640.197	3.818	639.387	3.517
667.443	3.488	640.357	3.756	639.707	3.563
667.613	3.475	640.837	3.781	640.027	3.576
667.923	3.479	650.846	3.659	640.197	3.509
668.083	3.454	651.006	3.659	640.357	3.483
668.553	3.446	651.166	3.659	640.517	3.471
668.722	3.425	651.326	3.605	641.327	3.454
669.032	3.442	651.486	3.622	650.846	3.266
669.192	3.429	651.645	3.592	651.166	3.257

Table I. *(Continued)*

T (K)	C_V (kJ · kg^{-1} · K^{-1})	T (K)	C_V (kJ · kg^{-1} · K^{-1})	T (K)	C_V (kJ · kg^{-1} · K^{-1})
651.326	3.303	616.469	3.262	744.291	2.102
651.486	3.257	616.669	3.257	$\rho = 74.11$ kg · m^{-3}	
651.645	3.232	617.029	3.278		
661.884	3.161	617.329	3.262	590.131	16.634[a]
662.044	3.165	617.489	3.262	590.301	16.203[a]
662.834	3.132	628.978	3.031	590.461	16.262[a]
663.004	3.128	629.148	3.048	590.791	16.333[a]
663.473	3.098	629.468	3.098	591.301	16.421[a]
676.781	2.922	630.128	3.065	591.631	16.550[a]
677.251	2.906	630.448	3.031	592.210	3.014
677.571	2.910	630.618	3.031	592.221	3.010
678.820	2.881	641.807	2.910	592.231	2.994
678.980	2.855	641.977	2.906	592.801	2.998
679.290	2.872	642.297	2.939	592.971	2.973
702.804	2.638	642.457	2.939	593.131	2.948
703.264	2.642	642.627	2.876	601.790	2.906
703.884	2.671	653.085	2.776	601.950	2.889
704.194	2.650	653.245	2.738	602.290	2.918
704.344	2.646	653.565	2.734	602.450	2.881
704.494	2.600	653.725	2.717	602.780	2.864
704.954	2.600	654.205	2.734	609.080	2.805
736.084	2.441	678.350	2.516	609.190	2.755
736.344	2.441	678.510	2.495	609.740	2.759
736.604	2.407	678.660	2.487	609.910	2.763
736.864	2.386	678.820	2.458	610.230	2.742
737.114	2.391	679.600	2.516	632.728	2.533
737.374	2.366	696.776	2.370	632.898	2.546
$\rho = 107.11$ kg · m^{-3}		696.936	2.399	633.218	2.512
		697.866	2.374	633.548	2.479
610.730	13.875[a]	698.016	2.353	633.868	2.504
610.890	13.875[a]	699.105	2.336	634.198	2.483
611.220	13.846[a]	699.415	2.361	659.964	2.303
611.390	13.862[a]	699.565	2.353	660.764	2.286
612.220	13.909[a]	719.869	2.186	660.924	2.319
612.540	13.950[a]	720.129	2.202	661.084	2.294
612.710	14.017[a]	720.379	2.186	661.404	2.303
613.365	3.337	720.639	2.244	661.564	2.257
613.380	3.308	720.899	2.227	697.866	2.081
613.530	3.303	721.159	2.223	698.016	2.102
614.190	3.324	743.272	2.152	698.176	2.052
614.360	3.274	743.521	2.114	698.326	2.039
615.180	3.266	743.781	2.144	740.283	1.951
615.350	3.257	744.041	2.093	740.542	1.951

Table I. *(Continued)*

T (K)	C_V (kJ · kg^{-1} · K^{-1})	T (K)	C_V (kJ · kg^{-1} · K^{-1})	T (K)	C_V (kJ · kg^{-1} · K^{-1})
740.802	1.934	575.151	2.675	630.778	2.156
741.062	1.926	576.671	2.700	631.108	2.098
741.322	1.888	576.841	2.688	631.258	2.156
741.482	1.913	577.181	2.684	671.892	1.951
$\rho = 52.47$ kg · m^{-3}		586.271	2.562	672.042	1.959
		586.431	2.554	672.202	1.934
570.061	17.995[a]	586.771	2.579	672.362	1.913
570.571	18.016[a]	587.111	2.575	672.522	1.926
570.741	17.991[a]	587.441	2.529	701.265	1.855
570.911	18.083[a]	587.611	2.520	701.565	1.867
571.081	18.070[a]	606.270	2.374	701.875	1.851
571.421	18.120[a]	606.440	2.361	702.194	1.821
571.761	18.112[a]	606.600	2.319	702.954	1.813
572.101	18.326[a]	606.930	2.353	703.114	1.825
572.675	2.755	607.260	2.315	740.452	1.750
572.681	2.747	630.118	2.165	741.482	1.775
573.451	2.713	630.288	2.119	742.502	1.750
573.801	2.696	630.448	2.131	743.521	1.712
574.981	2.692	630.618	2.102	744.547	1.775

[a] Two-phase experimental points.

where λ is the thermal conductivity of cuprous oxide ($\lambda \sim 2.09$ W · m^{-1} · K^{-1}), S is the surface area of the cuprous oxide layer, d is the thickness of the cuprous oxide layer, and $\Delta T = 10^{-4}$ K. The average time of one measurement was $\tau = 300$ s and the heat losses ΔQ for this time were ± 0.2 J, or 0.02% of the total heat supplied to the system. These parasitic energy losses were caused by operating problems of the temperature controller. It is straightforward to estimate heat losses through the areas of the calorimeter that are not controlled by the thermoelement (e.g., the well for the internal heater or the resistance thermometer). These losses did not exceed 4×10^{-4} J. Similar calculations of heat losses through the capillary used to fill the calorimeter with the sample yielded 3×10^{-3} J. Heat losses through the inlet and outlet wires of the internal heater were 0.066 J, and those through the wires of the temperature sensor, 0.0016 J. The heat flow through all uncontrolled areas was 0.27 J, or 0.06% of the total amount of heat supplied to the system.

Table II. Experimental Values of the Isochoric Heat Capacities of Heavy Water along the Saturation Boundary ($T_S = T_{S,exp} - 0.45$ K)

ρ_S (kg·m^{-3})	T_S (K)	C''_{V1} (kJ·kg^{-1}·K^{-1})	C''_{V2} (kJ·kg^{-1}·K^{-1})
52.4650	572.675	2.755	18.326
74.1120	592.205	3.015	16.551
107.112	613.365	3.337	14.018
170.387	632.200	3.773	13.458
219.298	639.580	4.274	13.569
261.097	643.150	5.252	14.105
303.030	643.650	6.513	15.059
338.409	643.720	7.845	18.966
344.828	643.840	8.131	19.436
ρ_S (kg·m^{-3})	T_S (K)	C'_{V1} (kJ·kg^{-1}·K^{-1})	C'_{V2} (kJ·kg^{-1}·K^{-1})
370.370	643.831	8.697	16.058
400.000	643.725	6.398	13.175
492.610	640.885	3.853	7.508
667.557	612.090	3.032	5.845
783.699	572.820	2.903	4.958
833.333	550.500	2.976	4.661
882.613	522.815	3.065	4.589
925.925	497.850	3.198	4.351
957.854	472.625	3.266	4.376
1008.07	431.685	3.444	4.226
1017.29	422.355	3.492	4.220
1063.83	371.100	3.756	4.216
1095.29	322.805	4.032	4.213
1104.97	294.805	4.185	4.262

The substance density also changed because of the temperature- and pressure-related changes of the calorimeter volume during heat capacity measurements. This means that the measurements were actually performed along quasi-isochores. In addition to these, other types of uncertainties must be considered which are associated with the uncertainties of determining the specific volume and temperature. The uncertainty of the experimentally determined C_V related to the uncertainty of the specific volume ΔV and temperature ΔT was calculated from the relation

$$\delta C_V = \frac{1}{C_V}\left(\frac{\delta C_V}{\partial V}\right)_T \Delta V + \frac{1}{C_V}\left(\frac{\partial C_V}{\partial T}\right)_V \Delta T \tag{12}$$

where ΔV and ΔT are the absolute uncertainties of the specific volume V and temperature T. The propagation of uncertainties related to the uncertainty of the specific volume for the liquid phase, where $(\partial C_V/\partial T)_V$ is small, yielded 0.04%. Near the critical point, where $(\partial C_V/\partial T)_V$ is large, the propagation of uncertainties yielded 0.06%. The uncertainties related to temperature were more substantial and reached 0.05% in the liquid phase and 0.25% near the critical point. Thus, the combined standard uncertainty related to the indirect measurement uncertainties did not exceed 0.5%.

Based on the detailed analysis of all sources of uncertainties likely to affect the determination of C_V with the present system, the combined standard uncertainty of measuring the heat capacity with allowance for the propagation of uncertainty related to the nonisochoric conditions of the process was 1.5% in the liquid phase, 3% in the vapor phase, and 4.5% near the critical point, where a normal distribution of errors is assumed and a coverage factor of 2 has been applied (equivalent to a confidence level of 95%).

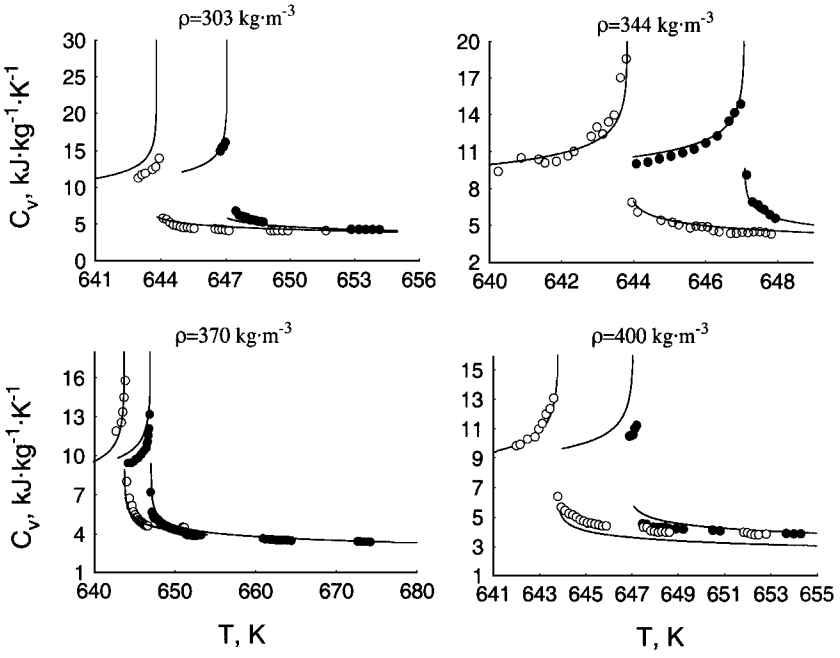

Fig. 2. One- and two-phase isochoric heat capacities of light and heavy water as a function of temperature at near-critical isochores. (○) D_2O (this work); (●) H_2O [7, 16–18, 22]; solid lines represent values of C_V calculated from the CR EOS.

The measurements were performed in both the forward direction (heating) and the reverse direction (cooling). The measured isochoric heat capacities were indeed independent of the direction. Differences of the experimental results were not more than $\pm 0.3\%$. The heavy water was 99.8% (by mass) pure, where the impurity was 0.2% (by mass) normal water.

This method, with some modifications in the calorimeter construction, has been used to measure the isochoric heat capacity of light water [7, 16–18], water + salt solutions [9, 18, 19], hydrocarbons [11, 20], alcohol [8], and carbon dioxide [10].

3. RESULTS AND DISCUSSION

Measurements of the isochoric heat capacity for heavy water (D_2O) were performed along 23 isochores: 52, 74, 107, 170, 219, 261, 303, 338, 345, 370, 400, 493, 668, 784, 833, 883, 926, 958, 1008, 1017, 1064, 1095, and 1105 $kg \cdot m^{-3}$. Each isochore consisted of 18 to 58 points. The temperature range was 294 to 746 K. In total, 786 C_V measurements were made, 153 in

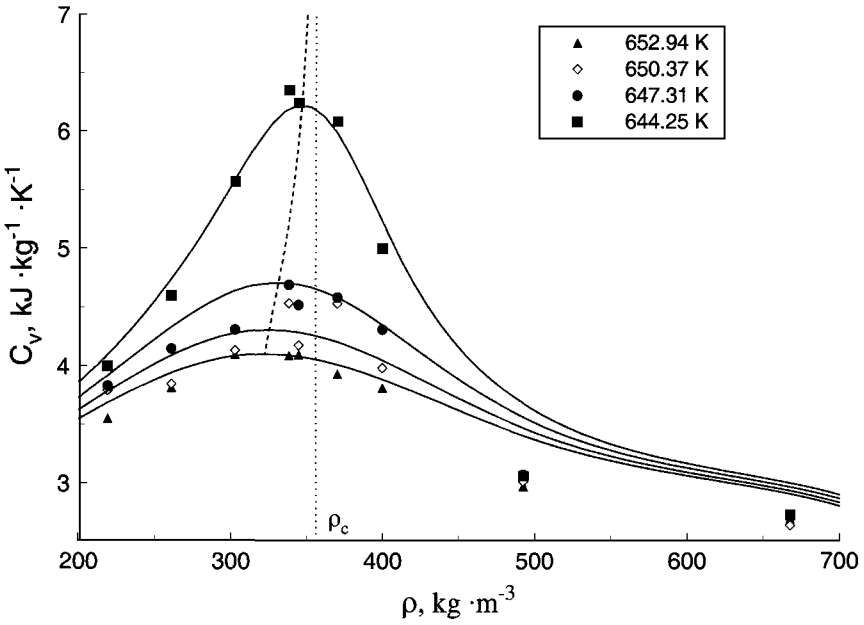

Fig. 3. Experimental values of C_V for heavy water as a function of density at supercritical isotherms. The solid lines represent calculated values of C_V at supercritical isotherms, and the dashed line represents the isothermal maximum loci of C_V calculated from the CR EOS.

the two-phase region and 633 in the one-phase region. Forty-six values of C_V were measured on the coexistence curve. The experimental values are given in Tables I and II. For each liquid and vapor isochore, the C_V measurements were made in the single- and two-phase regions, including liquid, vapor, subcritical, and supercritical states.

All experimental data for D_2O away from the critical point were compared with the Hill et al. [3] EOS and near the critical point

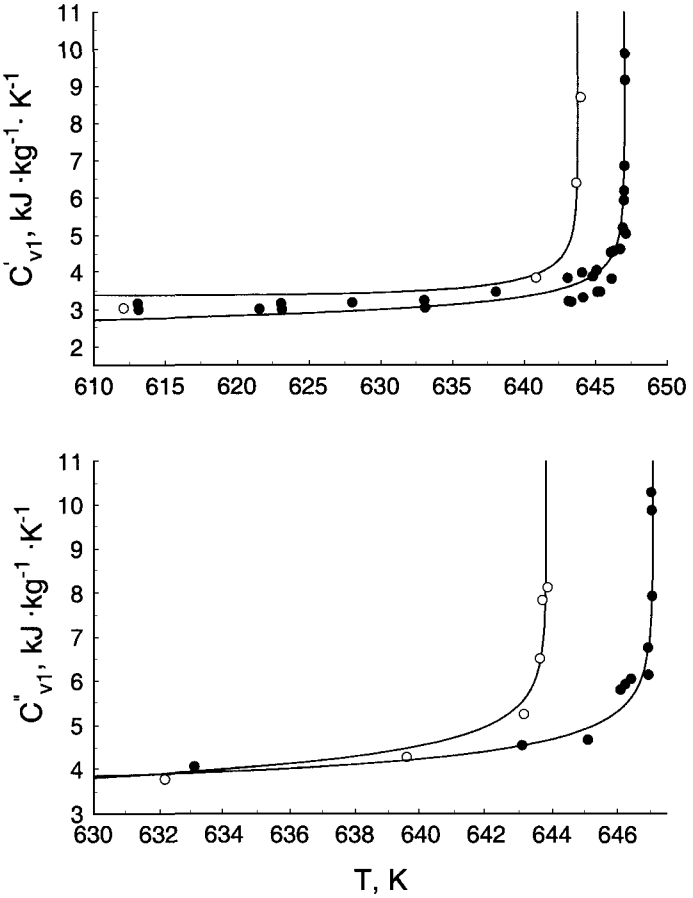

Fig. 4. Liquid (one-phase C'_{V1}) and vapor (one-phase C''_{V1}) isochoric heat capacities of light and heavy water as a function of temperature on the coexistence curve near the critical points. (○) D_2O (this work); (●) H_2O [7, 16–18, 22]; solid lines represent values of C_V calculated from the CR EOS.

with the crossover equation of state (CR EOS) [5]. Figure 2 shows the experimental behavior of C_V as a function of temperature for D_2O and H_2O [7, 16–18, 22] at various near-critical isochores. The crossover equation of state of Kiselev and Friend [23] was used to calculate the properties of H_2O. The density dependence of C_V for heavy water along supercritical isotherms ($T = 652.94$, 650.37, 647.31, and 644.25 K) is shown in Fig. 3. The values of liquid and vapor one-phase (C'_{V1}, C''_{V1}) and two-phase (C'_{V2}, C''_{V2}) isochoric heat capacities on the coexistence curve for heavy

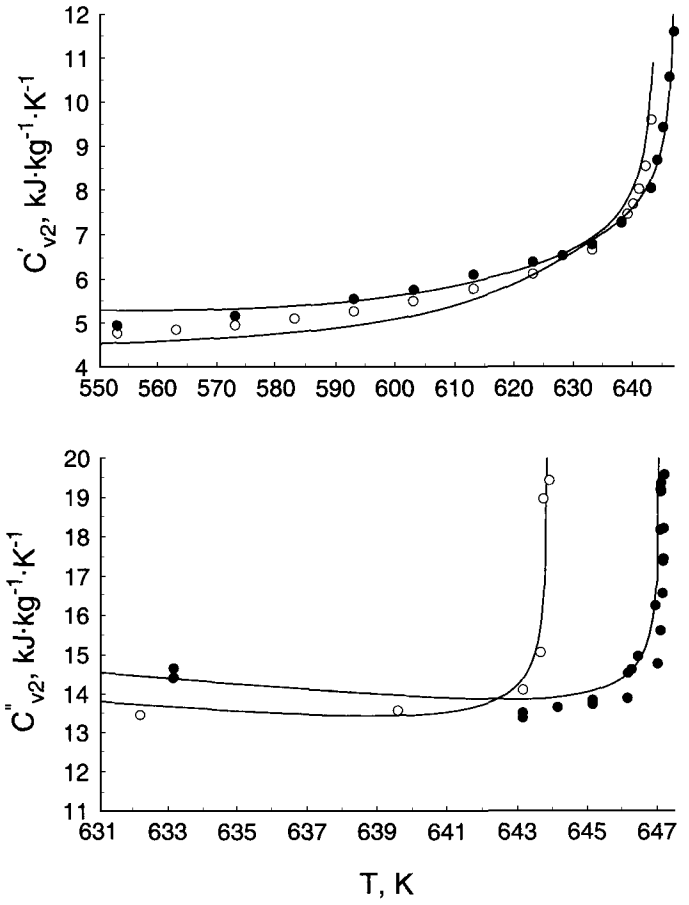

Fig. 5. Liquid (two-phase C'_{V2}) and vapor (two-phase C''_{V2}) isochoric heat capacities of light and heavy water as a function of temperature on the coexistence curve near the critical points. (○) D_2O (this work); (●) H_2O [7, 16–18, 22]; solid lines represent values of C_V calculated from the CR EOS.

water are shown in Figs. 4 and 5 together with light water results. Figure 6 shows experimental results for the isochoric heat capacity jumps of D_2O and H_2O for the liquid ($\Delta C'_V$) and vapor ($\Delta C''_V$) isochores. The experimental results of temperatures and densities along the coexistence curve which were determined from C_V experiments for heavy and light water are presented in Table II and Fig. 7. The experimental values of the two-phase heat capacity C_V as a function of the volume along the coexistence curve are presented in Fig. 8.

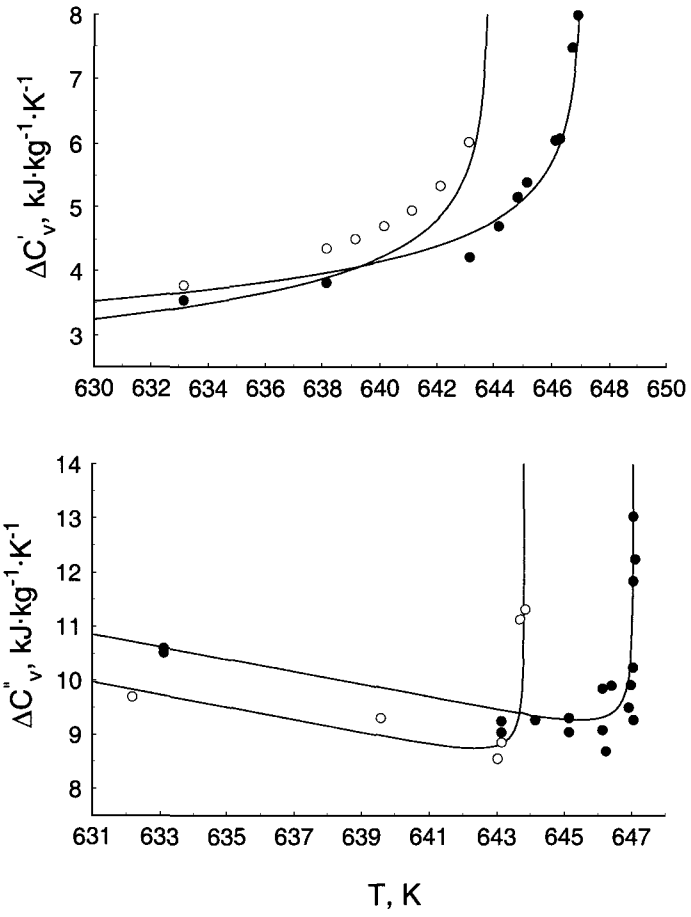

Fig. 6. Liquid ($\Delta C'_V$) and vapor ($\Delta C''_V$) isochoric heat capacity jumps for light and heavy water as a function of temperature near the critical points. (○) D_2O (this work); (●) H_2O [7, 16–18, 22]; solid lines represent values of C_V calculated from the CR EOS.

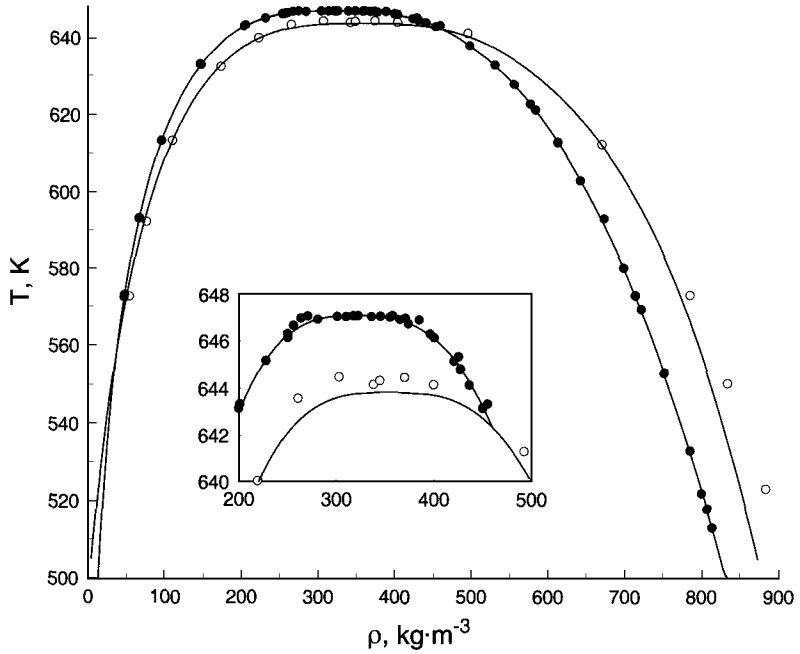

Fig. 7. Curves of coexisting liquid and vapor densities for light and heavy water from C_V experiments near the critical points. (○) D_2O (this work); (●) H_2O [7, 16–18, 22]; solid lines represent values of C_V calculated from the CR EOS.

The results of comparisons with the Hill EOS are presented in Figs. 9 and 10 for several liquid and vapor isochores. Deviation plots for all isochores except those at 303, 338, 370, and 400 $kg \cdot m^{-3}$ are given in Fig. 11. Several near-critical points ($T < 650$ K) for the 345 $kg \cdot m^{-3}$ isochore were also removed. The Hill EOS represents the data shown in Fig. 11 with an average absolute deviation of 3.1% and a bias of −2.3%. Several isochores show systematic deviations up to 12%. The one-phase C_V data for the liquid isochores 1017, 1064, 1095, and 1105 $kg \cdot m^{-3}$ are generally represented by the Hill EOS within 1.8%, which is slightly higher than the experimental uncertainty. Most of the data for the liquid isochores show that experimental values of C_V are systematically lower than the calculated values as the temperature increases away from the saturation temperature. Nevertheless, the deviations are still close to their experimental uncertainties. These trends tend to increase for the isochores from 833 to 958 $kg \cdot m^{-3}$, up to a maximum of −9.2%.

The agreement between experimental data and the Hill EOS in the vapor phase is generally about the same as in the liquid phase. For the

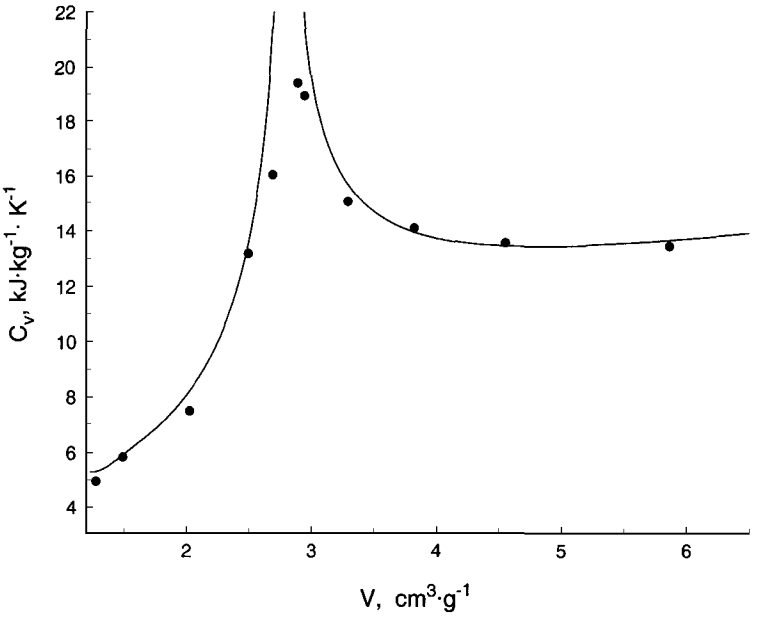

Fig. 8. Two-phase isochoric heat capacities of heavy water as a function of specific volume at the coexistence line. (●) experimental values of C_V along the coexistence line; solid lines represent values of C_V calculated from the CR EOS.

vapor isochores at 170 and 219 kg·m^{-3}, the deviations are on average about 2.8%, which are within the experimental uncertainty. Generally, for these isochores, the experimental C_V values are less than the calculated values. For the vapor isochore at 261 kg·m^{-3}, deviations are again negative at the higher temperatures; however, near saturation, the deviations approach 10% due to the influence of critical phenomena. For the lowest density isochores, the uncertainty increases as the amount of mass in the apparatus becomes small. Due to this, deviations may exceed −10% at the lowest density and highest temperatures.

The experimental C_V data include eight near-critical isochores: 219, 261, 303, 338, 345, 370, 400, and 493 kg·m^{-3}. Comparisons of the isochoric heat capacity measurements near the critical point with the CR EOS are given in Fig. 2. Good agreement between experimental and calculated values of C_V in the two-phase region is observed for most of the isochores. Deviations are on average about 2%, which is considerably lower than their uncertainty. For all near-critical isochores at temperatures near the phase transition temperatures [from $T_S(\rho)$ to $T_S(\rho)+2$ K], the experimental values of C_V are represented by the CR EOS within 15%.

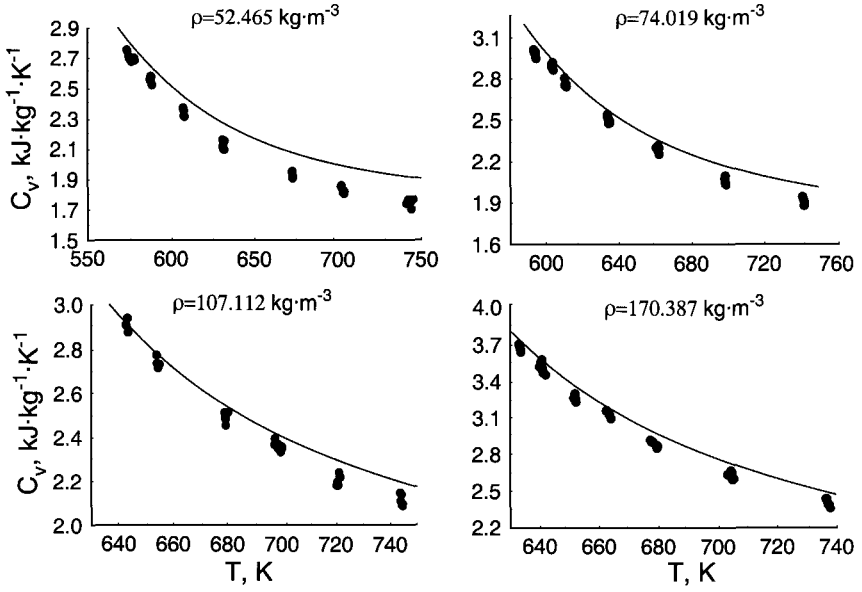

Fig. 9. Comparison of experimental isochoric heat capacity values of heavy water with values calculated from the KS EOS for vapor isochores far from the critical point.

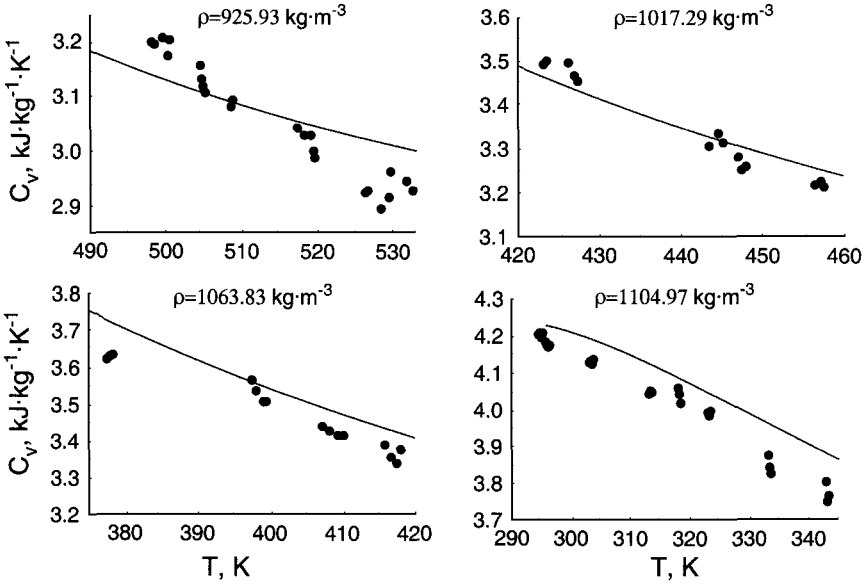

Fig. 10. Comparison of the experimental isochoric heat capacity values of heavy water with values calculated from the Hill EOS for liquid isochores far from the critical point.

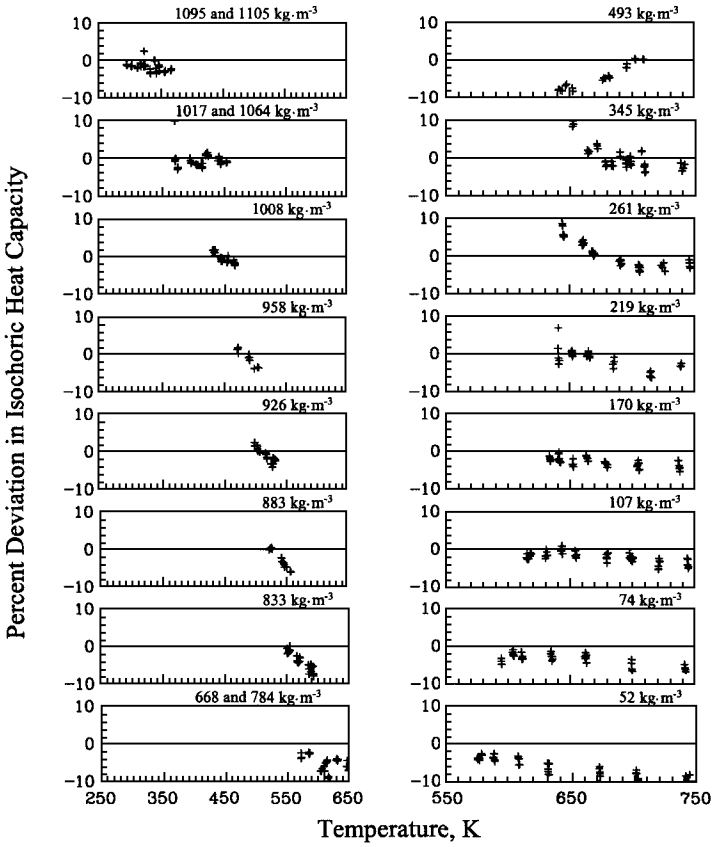

Fig. 11. Percentage deviations of experimental isochoric heat capacity data for heavy water from values calculated with the Hill EOS for liquid and vapor isochores.

Good agreement (within 2%) is observed for the isochores at 303 and 344 $kg \cdot m^{-3}$ in the temperature range from $T_S(\rho)$ to 740 K. Only 5 points out of 90 show deviations of about 10%.

The CR EOS was developed using experimental PVT, vapor pressure, and C_V data. The crossover model showed that the value of T_c (643.847 K, ITS-90) reported by Blank et al. [24] and recommended by Levelt Sengers (IAPWS formulation) [25] was in very good agreement with other measurements. However, the value of T_c (644.34 K) obtained by Mursalov from his C_V measurements was 0.493 K higher than the recommended value. Additionally, the saturation temperatures for near critical isochores determined from C_V measurements showed that the experimental values were on average 0.45 K too high when compared with the crossover model (see Fig. 7). The

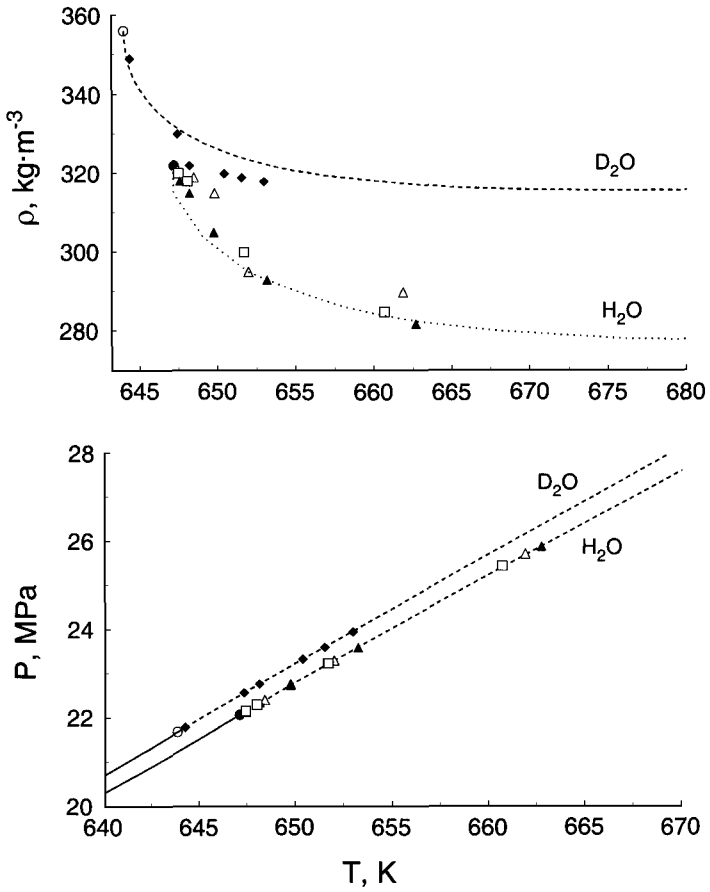

Fig. 12. Locus of supercritical isothermal maxima of C_V on the temperature–density and pressure–temperature planes for light and heavy water near the critical points. (○) critical point of D_2O; (●) critical point of H_2O; dashed line represents the loci of isothermal maxima of C_V calculated from the CR EOS; (◆) D_2O (this work); (□) H_2O [7]; (△) H_2O [16]; (▲) H_2O [22].

most probable cause of this systematic error is due to an impurity left over from the preparation of the calorimeter before the measurements began. Therefore, the original values for the experimental temperatures were adjusted down by 0.45 K. Because this shift cannot be justified by artifacts in the experimental measurements, it is arbitrary and subject to change. The major justification is that it brings the data into agreement with calculations from an accurate crossover model for which the T_c is assumed

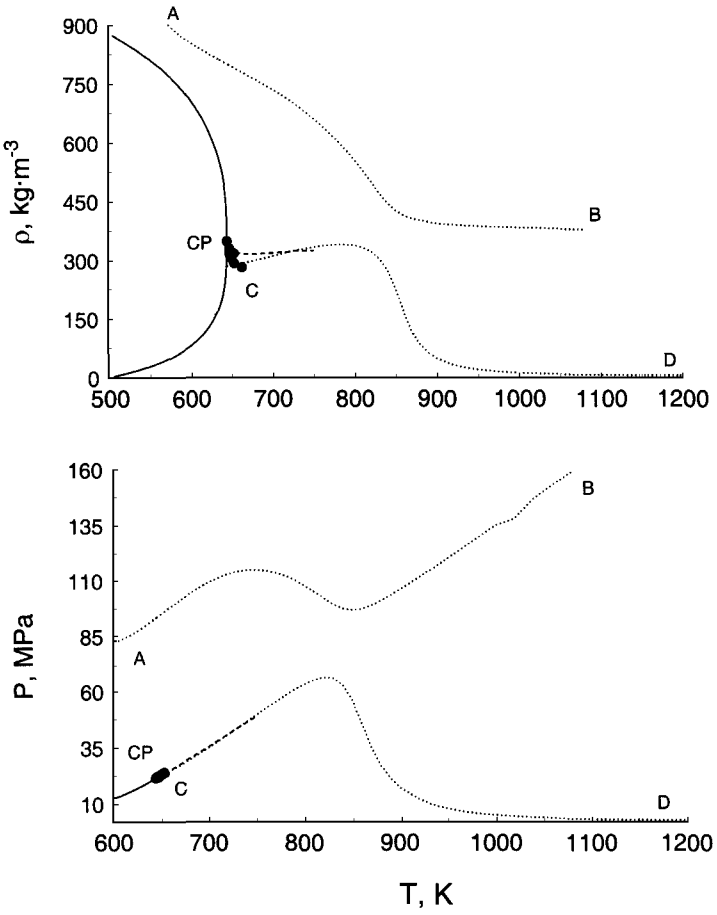

Fig. 13. Loci of isothermal-maxima (line CD) and minima (line AB) of C_V on the temperature–density and pressure–temperature planes for heavy water predicted by the Hill EOS (·····) [4] and the CR EOS (-----) [23]. (●) isothermal maxima of C_V from experiment.

to be reliable. New measurements are required to establish the validity of this shift and the data in the critical region should be used with caution until new measurements are carried out and comparisons are made with this study. *The adjusted numbers are reported in Tables I and II.*

Because the isochoric heat capacity and density near the critical point change rapidly (dC_V/dT and $d\rho_S/dT$ are large) with temperature, even small deviations in temperature result in large deviations in C_V and ρ_S. The adjustments due to the temperature shift are negligible at densities and temperatures far from the critical point where values of the derivatives

dC_V/dT and $d\rho_S/dT$ are small. After temperature adjustments were applied, deviations between experimental values of C_V and the CR EOS decreased by up to 5 to 6%, which is close to the experimental uncertainties. The original experimental saturation densities extracted from C_V experiments after applying the temperature adjustment are in good agreement with the CR EOS.

The temperature dependence of deviations of experimental data near the critical point is given in Fig. 12. Figure 13 shows comparisons of the isothermal maximum loci of the isochoric heat capacity in the supercritical region with values predicted from the CR EOS. Figure 13 also shows comparisons of the loci of isothermal maxima and minima of C_V for heavy water predicted from the Hill EOS and the CR EOS in the T–ρ and P–T planes. The Hill EOS does not predict isochoric minima of C_V which have been experimentally observed.

4. CONCLUSIONS

The results of the isochoric heat capacity measurements of heavy water in the temperature range from 294 to 746 K and at densities between 52 and 1105 $kg \cdot m^{-3}$ are reported. These measurements include the subcritical and supercritical regions. The measurements are described by the crossover equation of state, which is valid in the extended critical region ($0.8 \leqslant T/T_c \leqslant 1.5$ and $0.35 \leqslant \rho/\rho_c \leqslant 1.65$). The results of the isochoric heat capacity measurements are in good agreement with the crossover model. All original experimental data were lowered by 0.45 K and the data in the critical region should be used with caution until additional experimental data validate this arbitrary adjustment.

ACKNOWLEDGMENTS

The authors thank J. W. Magee for many valuable discussions during this work. S.B.K. and I.M.A. also thank the Physical and Chemical Properties Division at the National Institute of Standards and Technology for the opportunity to work as Guest Researchers at NIST during the course of this research. Part of this work was also supported by the Russian Science Foundation under Grants 96-02-16005 and INTAS-96-1989.

REFERENCES

1. B. A. Mursalov, Ph.D. dissertation (AZNEFTEChIM, Baku, Azerbaidzhan, USSR, 1973).
2. Kh. I. Amirkhanov, G. V. Stepanov, B. A. Mursalov, and O. A. Bui, *Teploenergetika* **22**:68 (1973).
3. P. G. Hill, R. D. C. MacMillan, and V. Lee, *J. Phys. Chem. Ref. Data* **11**:1 (1982).

4. J. Kestin and J. V. Sengers, *J. Phys. Chem. Ref. Data* **15**:305 (1986).
5. S. B. Kiselev, I. M. Abdulagatov, and A. H. Harvey, *Int. J. Thermophys.* **20**:563 (1999).
6. Kh. I. Amirkhanov, Ph.D. dissertation (University of Leningrad, Leningrad, 1948).
7. Kh. I. Amirkhanov, G. V. Stepanov, and B. G. Alibekov, *Isochoric Heat Capacity of Water and Steam* (Amerind, New Delhi, 1974).
8. Kh. I. Amirkhanov, G. V. Stepanov, I. M. Abdulagatov, and O. A. Bou, *Isochoric Heat Capacity of Propanol and Isopropanol* (Makhachkala, Dagestan Scientific Center of the Russian Academy of Sciences, 1989).
9. I. M. Abdulagatov, V. I. Dvoryanchikov, and I. M. Abdurakhmanov, *Proc. 11th Int. Conf. Prop. Water Steam*, M. Pichal and O. Sifner, eds. (Hemisphere, New York, 1989), pp. 203–209.
10. I. M. Abdulagatov, N. G. Polikhronidi, and R. G. Batyrova, *Ber. Bunsenges. Phys. Chem.* **98**:1068 (1994).
11. I. M. Abdulagatov, S. B. Kiselev, L. N. Levina, Z. R. Zakaryaev, and O. N. Mamchenkova, *Int. J. Thermophys.* **17**:423 (1996).
12. V. A. Kirilin and A. E. Sheidlin, *Fundamentals of Experimental Thermodynamics* (Moscow, 1948).
13. U. M. Porovskii and B. V. Deragin, *Dokl. AN USSR* **159**:897 (1964).
14. A. C. Bestujeva, Ph.D. dissertation (MPI, Moscow, 1968).
15. Z. R. Zakar'yaev, Ph.D. dissertation (IGR DSC RAS, 1995).
16. I. M. Abdulagatov, B. A. Mursalov, and N. M. Gamzatov, *Proc. 12th Int. Conf. Prop. Water Steam*, H. White, J. V. Sengers, D. B. Neumann, and J. C. Bellows, eds. (Begell House, New York, 1995), pp. 94–102.
17. I. M. Abdulagatov, V. I. Dvoryanchikov, and A. N. Kamalov, *J. Chem. Eng. Data* **43**:830 (1998).
18. I. M. Abdulagatov, V. I. Dvoryanchikov, and A. N. Kamalov, *J. Chem. Thermodyn.* **29**:1387 (1997).
19. I. M. Abdulagatov, V. I. Dvoryanchikov, B. A. Mursalov, and A. N. Kamalov, *Fluid Phase Equil.* **143**:213 (1998).
20. I. M. Abdulagatov, L. N. Levina, Z. R. Zakaryaev, and O. N. Mamchenkova, *Fluid Phase Equil.* **127**:205 (1997).
21. I. M. Abdulagatov and V. I. Dvoryanchikov, *J. Chem. Thermodyn.* **25**:823 (1993).
22. A. M. Kerimov, Ph.D. dissertation (AZNEFTEChIM, Baku, Azerbajdzgan, USSR, 1964).
23. S. B. Kiselev and D. G. Friend, *Fluid Phase Equil.* **155**:33 (1999).
24. G. Blank, *Warme und Stoffubertragung* **2**:53 (1968).
25. J. M. H. Levelt Sengers, J. Straub, K. Watanabe, and P. G. Hill, *J. Phys. Chem. Ref. Data.* **14**:193 (1985).